M. H. Wu
Research Assistant

W. Hsu
Professor

Department of Mechanical Engineering
National Chiao Tung University
Hsin Chu, Taiwan 300, ROC

Investigation of Torsion Springs by Considering the Friction and the End Effect

In this study, the nonlinearity in moment and angular displacement of torsion springs is studied analytically and experimentally. It is shown that the inclined angles at both ends have direct effects on the nonlinearity of a constant-pitch torsion spring. Also, an algorithm for determining the friction between the spring coils in close-wound torsion springs is proposed. From the comparison to experimental data, it is found that the spring rates are different at forward and backward strokes. The dynamic equations for the close-wound torsion spring is also derived by considering the friction between the spring coils, and two different natural frequencies are found in simulation.

Introduction

Helical torsion springs are very common components in mechanical systems. In the early years, most of the studies of torsion springs focused on stresses, deflections, curvature changes, diametrical contractions and coupling effects.

Gohner's [1, 2] discussed the ideal case of torsion springs for the stresses and the displacements with zero pitch. Berry [3] measured the angular deflections of many torsion springs and discovered that the deflections were considerably larger than those predicted from the linear formation. Ancker and Goodier [4, 5] derived equations to obtain deformations and stresses by considering both pitch and curvature. They also proposed the diametrical contraction of the torsion spring. However, those deflection formulation are still linear.

Manos [6] designed a torsion spring with variable spring rate. Carlson [7] observed that the compression spring with ends squared and ground often tiped several degrees to one side when compressed. For this reason, the compression springs will buckle much quicker under compression. Recently, Rouch and Bruner [8] analysed helical springs under loading which caused large deformations to have nonlinear moment-deflection relation by using the helical finite element method. Wu et al. [9] discussed the nonlinearity of compression helical springs caused by the coil close and the friction due to the damper.

The torsion spring often exhibits a nonlinear moment-deflection relationship even under small deformations. Also, for close-wound torsion springs, i.e. the spring coils are in contact with each other, the friction between spring coils directly affects the performance of torsion springs. Therefore, a nonlinear hysteresis loop in the moment-deflection curve of a torsion spring becomes very typical.

However, the algorithm of determining the friction and nonlinearity of moment-deflection curve in torsion springs were not discussed in previous literature. In this study, we propose a theoretical formulation to obtain the moment-deflection curve in the helical torsion springs by considering the friction force due to spring coils contact and inclined angles at both ends with experimental verification. Two types of helical torsion springs are discussed, a helical close-wound torsion spring with friction, and a torsion spring with constant pitch and inclined ends.

Moment-Deflection Relation with Inclined Ends

The deflection for a torsion spring from elementary theory is

$$\phi = \frac{ML}{EI} \tag{1}$$

where ϕ denotes the total angular displacement of the torsion spring, M represents the applied torque, E denotes the elastic module of the spring material, L represents the total helical length, and I is the moment of inertia of the spring wire.

Berry [3] measured the angular deflections of many torsion springs and discovered that the deflections were considerably larger than those predicted from Eq. (1) which has been developed without taking into account the curvature of the wire. Berry found that the angular deflection should be increased slightly. Then, Goodier and Ancker [5] proposed the relationship between the moment and the angular displacement of the torsion spring as

$$\phi = \frac{ML}{EI} \psi \tag{2}$$

for Poisson ratio $v = 0.3$,

$$\psi = 1 - 0.018 \left(\frac{d}{2R}\right)^2 + 1.3 \tan^2 p + \ldots \tag{3}$$

where d is the wire diameter, and p is pitch angle. Also, R is the mean coil radius in loading and is given by:

$$R = R_0 + \frac{64MR_0^2}{\pi d^4 E}$$

$$\times \left[-1 + 0.30711 \left(\frac{d}{2R_0}\right)^2 + \tan^2 p + \ldots \right] \tag{4}$$

where R_0 denotes the mean coil radius without loading.

When there is an inclined angle θ_0 in the $Y - Z$ plane at both ends of a torsion spring, the applied torsion moment M_R along Z-axis can be divided into a bending moment M_1 and a torsion moment M_2 as shown in Fig. 1. The bending moment M_1 which is perpendicular to the central axis of the spring coil can be expressed as

$$M_1 = M_R \sin \theta_0 \tag{5}$$

Since the bending moment M_1 is in the $Y' - Z'$ plane, the angular deflection θ_1 caused by the moment M_1 will be in the $X' - Z'$ plane, as shown in Fig. 2. The moment M_1 can be separated into a torsion component $M_1 \cos \varphi$ tangent to the spring wire axis and a bending component $M_1 \sin \varphi$ perpendicular to the spring wire axis. It is assumed that the helix angle is small so that the
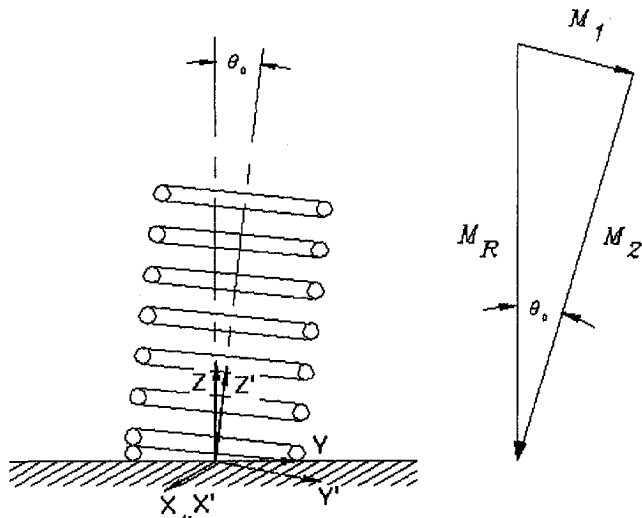
Fig. 1 The inclined angle θ_0 at the ends of the torsion spring

moment vector lies in a plane perpendicular to the center axis of the spring coil. For a small element of length $Rd\varphi$, the bending component produces an angular deflection

$$\frac{M_1 R \sin \varphi d\varphi}{EI} \qquad (6)$$

and the torsion component produces a rotation

$$\frac{M_1 R \cos \varphi d\varphi}{GJ_s} \qquad (7)$$

The central axis of the spring coil deflects in a plane perpendicular to the resultant moment vector M_1. Other deflection tends to cancel out. Taking the components of the deflection contributions in that plane and integrating over the entire spring, we obtain

$$\theta_1 = M_1 R \int_0^{2\pi n} \left(\frac{\sin^2 \varphi}{EI} + \frac{\cos^2 \varphi}{GJ_s} \right) d\varphi$$

$$= M_R \sin \theta_0 R \left(\frac{n\pi - \frac{1}{4} \sin 4n\pi}{EI} + \frac{n\pi + \frac{1}{4} \sin 4n\pi}{GJ_s} \right) \qquad (8)$$

where I represents the moment of inertia of the wire cross section, J_s represents the polar moment of inertia for spring wire cross section, n is the number of active coils, and G denotes the shear module of the spring material.

Because of the angular deflection θ_1 and the inclined angle θ_0 are in the different planes, the resultant bending moment M_B (Fig. 3) becomes

$$M_B = M_R \sqrt{\sin^2 \theta_1 + \sin^2 \theta_0} \qquad (9)$$

and the resultant torsion component M_T is

$$M_T = (M_R^2 - M_B^2)^{1/2}$$

$$= M_R (\cos^2 \theta_1 - \sin^2 \theta_0)^{1/2} \qquad (10)$$

Then from Eq. (2), the torsion moment M_T produces an angular displacement ϕ as

$$\phi = \frac{M_T L}{EI} \psi \qquad (11)$$

From Eq. (10) and (11), it can be seen that the relation between ϕ and M_R is nonlinear.

Friction Force

Since the angular displacement ϕ can not be very large for the close-wound torsion spring, the effect caused by the inclined angle θ_0 is negligible in that case. However, spring coils are in contact with each other for a close-wound torsion spring, therefore, friction force must be considered.

In order to formulate the friction force in a close-wound torsion spring, we must derive the normal force between the spring coils. The vertical displacement δ_1 of a point on the spring helix under a torsion moment M_T proposed by Ancker and Goodier [5] is

$$\delta_1 = \frac{128 M_T R^2 n \tan p \upsilon}{E d^4} \qquad (12)$$

where υ denotes the Poisson ratio, p is the pitch angle, and spring coils are not necessarily in contact.

When spring coils are in contact, the torsion spring will wind up and the number of active coils increases. Because the spring coils are still in contact with one another for a close-wound torsion spring, a vertical displacement δ_2 will be formed due to the wind-up phenomenon as
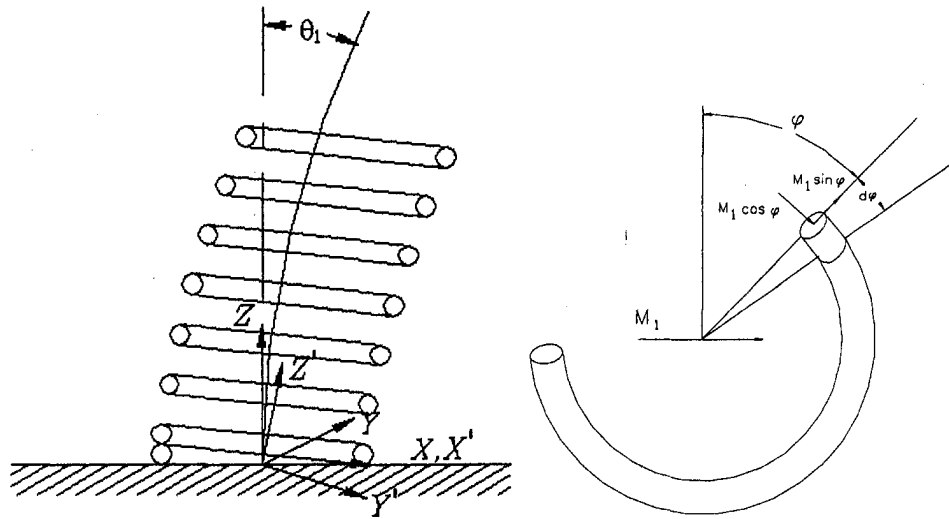
Nomenclature

d = diameter of the spring wire
E = elastic module of the spring material
F_f = the total frictional force
G = shear module of the spring material
I = moment of inertia for spring wire cross section
J = polar moment of inertia of the disk
J_s = polar moment of inertia for spring wire cross section
K = tensional spring rate
k_t = torsional spring rate
L = total helical length
M = the applied torque
M_B = resultant bending moment
M_C = constant frictional torque in the system

M_f = total frictional torque
M_R = applied torque along Z axis
M_s = friction torque due to the testing system
M_T = resultant torsion moment
M_1 = bending moment resulted from M_R
M_2 = torsion moment resulted from M_R
N = total normal force on spring wires
N_i = initial normal force on spring wires due to preload
n = number of the active coils
n_p = increasing number of the active coils
p = pitch angle
R = mean coil radius in loading
R_0 = initial mean coil radius

θ_0 = inclined angle at spring ends
θ_1 = deflection angle due to moment M_1
ϕ = angular displacement of the torsion spring
ϕ_0 = initial angular displacement
ψ = correction factor for angular displacement due to pitch angle
φ = angular position of the spring wire
δ_1 = vertical displacement resulted from M_T
δ_2 = vertical displacement resulted from wind-up
μ = dynamic friction coefficient
υ = poisson ratio
ω_{n1} = the frequency in the load increasing stroke of the torsion spring
ω_{n2} = the frequency in the load decreasing stroke of the torsion spring

Fig. 2 The angular deflection θ_1 caused by the moment M_1

$$\delta_2 = n_p \times d = \frac{\phi \times d}{2\pi} \tag{13}$$

where n_p denotes the increasing of the number of the active coils when loaded, d is the diameter of the spring wire, and ϕ is the angular deflection of the spring in radian.

The free-body diagram of the coil segment of a close-wound torsion spring is shown in Fig. 4, where N_i is the initial normal force acting on the spring wires due to the preloading, and K is the tensional spring rate of the close-wound torsion spring, p is the pitch angle, and F_1 denotes the force supplied by the input torsion moment M_T. Then the total normal force acting on the spring wire becomes

$$N = F_1 \sin p + N_i + K(\delta_1 + \delta_2) \cos p$$

$$= \frac{M_T}{R} \sin p + N_i + \frac{Gd^4}{64R^3(n + n_p)}$$

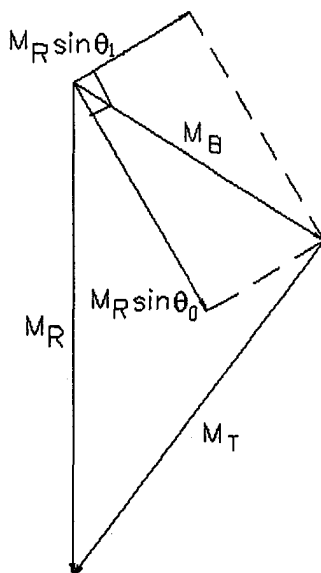$$\times \left(\frac{128 M_T R^2 n \tan pv}{Ed^4} + n_p \times d \right) \cos p \tag{14}$$

Fig. 3 Moment analysis diagram for M_r, M_B, and M_T

The total friction force F_f between spring coils then becomes

$$F_f = \mu N(n + n_p - 1) \tag{15}$$

where μ is the friction coefficients between spring coils.

So the total friction torque can be expressed as

$$M_f = R \times F_f \cos p + M_s \tag{16}$$

where M_s is a constant friction torque due to the testing system.

Then from Eq. (11) and (16), the moment-deflection relation including the coulomb friction becomes

$$M = M_R + M_f = \frac{\phi EI}{\psi L \sqrt{(\cos \theta_1^2 - \sin \theta_0^2)}}$$

$$+ M_s \, \text{sgn} \, (\dot{\phi}) + R \times F_f \cos p \, \text{sgn} \, (\dot{\phi}) \tag{17}$$

where M denotes the total input moment required to have angular deflection ϕ. The last term of friction moment exists only for the close-wound torsion spring, where the coils are in contact with each other.

Static Experimental Verification

A schematic diagram of the test facility is shown in Fig. 5. The test setup consists of the input shaft with the torsion spring, the fixed shaft, the power screw, and the rack and pinion.

In the experimental setup, the torsion spring is placed between the input shaft and fixed shaft, and the input shaft is driven by the
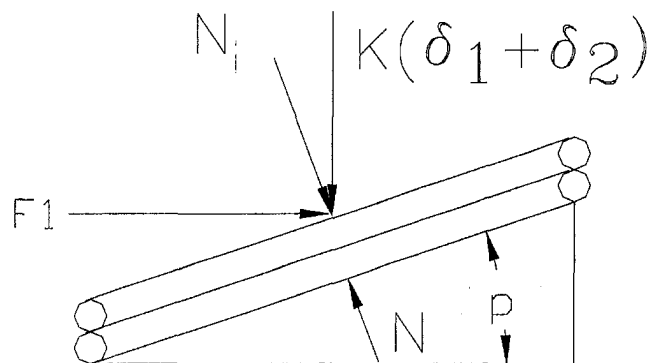

Fig. 4 The free body diagram of the middle region of the closed-wound torsion spring
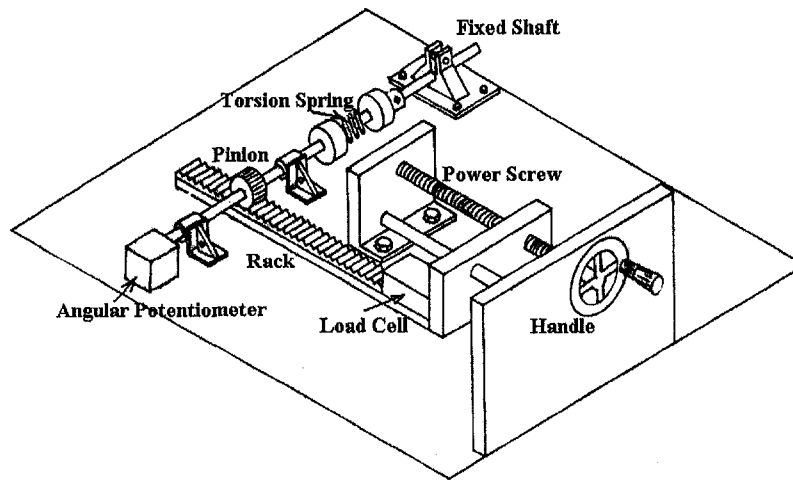
Fig. 5 The torsion spring experimental setup

pinion. The rack will drive the pinion when the handle is rotated. The load cell is used to measure the force acting on the rack, and the angular potentiometer mounted on the end of the input shaft can measure the angular displacement of the input shaft. Then the moment-deflection curve for the torsion spring can be obtained.

4.1 Constant-Pitch Torsion Spring. Here a constant-pitch torsion spring is tested to verify Eq. (17). Since the spring coils are not in contact with each other, the last term in Eq. (17) is set to zero. The parameters of the torsion spring are calibrated and listed in Table 1.

The experimental and simulated results for the constant-pitch torsion spring are shown in Fig. 6. The torsion spring is rotated forward first, then released slowly back to the initial position.

Table 1 Parameters for the constant-pitch torsion spring

Symbol	Description	Value
n	Number of the active coil	9.8
E	Elastic module of spring material	180 Gpa
ν	Poisson ratio	0.3
R_0	Initial mean coil radius	5.595 mm
d	Spring wire diameter	1.38 mm
θ_0	Inclined angle at spring ends	6.8 deg

Since there are inclined angles at both ends, the effect of an angular deflection θ_1 due to the bending moment must be considered. Fig. 6 reveals an evident nonlinearity at large rotation angles. The gap between forward and backward curves comes from the friction between spring wires and supporting shaft, and this frictional torque is almost constant. The maximum error between simulation and experimental results is about 2.083 Kg-mm. If the end effect is ignored, shown in Fig. 7, a large error (about 19.8177 Kg-mm) can be found between the linear model and experimental data. It indicates that the torsion spring with inclined ends can provide a larger stiffness, together with friction, then the maximum stress in the spring wire will be elevated, especially at large rotation angles, which may reduce the life of the spring.

4.2 Close-Wound Torsion Spring. Parameters of a close-wound torsion spring are calibrated and listed in Table 2. Since the coils are in contact here, the friction force becomes very important.

To determine the friction coefficient between the spring coils. Two identical torsion springs are placed on a horizontal plate by placing one spring above another at rest. Then the plate is tilted slowly until the top spring slides down at the tilt angle α. Then the friction coefficient μ between the spring wires in contact is tan α. With this rough approximation, here the friction coefficients is found to be 0.28 without lubricating.

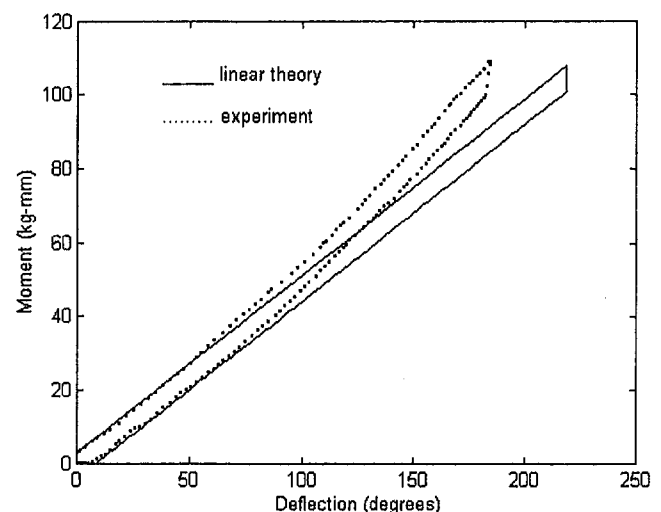The moment-deflection data are also taken on the static torsion

Fig. 6 The load-deflection curve of torsion spring of constant pitch with inclined ends

Fig. 7 The linearity of load-deflection curve of torsion spring with constant pitch

Table 2 Parameters for the close-wound torsion spring

Symbol	Description	Value
n	Number of the active coils	5.6
E	Elastic modules of spring material	180 Gpa
ν	Poisson ratio	0.3
R_0	Initial mean coil radius	9.7 mm
d	Spring wire diameter	1.6 mm
p	Pitch angle	4 deg
μ	Friction coefficient between the spring wires	0.28

test station which records the applied moment under the given angular displacement. Fig. 8 summarizes the results of Eq. (17) and experimental data for the close-wound torsion spring. It is found that the friction force due to the spring wires dramatically changes the spring torque. Also the gap between upper and lower curves increases with the angular deflection, which can be found in both simulation and experimental data. The upper curve in simulation is almost identical to the experimental data, however even the trend is similar, the maximum difference between simulation and calibrated data at lower curves is about 7 kg-mm. It is found that the spring rates are different at forward and backward strokes.

Dynamic Equation for A Close-Wound Torsion Spring

In a close-wound torsion spring, the direction of the friction torque depends on the angular velocity of spring coils. Therefore, for the model shown in Fig. 9, the equation of motion is equivalent to the following two linear equations:

$$\dot{\phi} \geq 0:\ J\ddot{\phi} + k_t\phi = -M_c - c\phi \tag{18}$$

$$\dot{\phi} \leq 0:\ J\ddot{\phi} + k_t\phi = M_c + c\phi \tag{19}$$
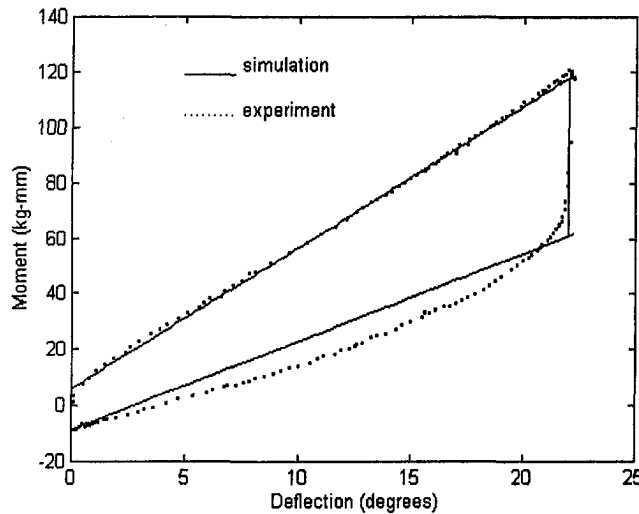

Fig. 8 The moment-deflection curve of the close-wound torsion spring
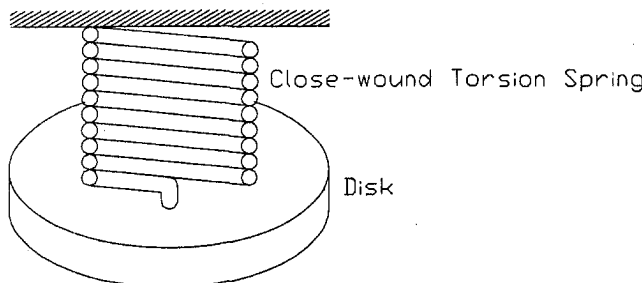

Fig. 9 Vibration mode of the torsion spring

where k_t represents the torsion stiffness of the torsion spring, J is the moment of inertia of the disk, and $M_c + c\phi$ represent the friction torque. Also the initial position $\phi = \phi_0$ and initial velocity $\dot{\phi}_0 = 0$ are specified. Where M_c is constant, and neglect the radial contraction the increase of the number of the active coil are neglected, and

$$c = \mu R\left[\frac{EI\sin p}{RL\psi} + \frac{Gd^4}{64R^3 n}\left(\frac{128IR^2 n\tan pv}{d^4 L\psi} + \frac{d}{2\pi}\right)\right](n-1)$$

$$= \text{constant}$$

for the constant-pitch torsion spring, $c = 0$.

Then the general solution becomes

$$\dot{\phi} \geq 0:\ \phi = A_+\cos \omega_{n1}t + B_+\sin \omega_{n1}t - a_+ \tag{20}$$

$$\dot{\phi} \leq 0:\ \phi = A_-\cos \omega_{n2}t + B_-\sin \omega_{n2}t + a_- \tag{21}$$

where

$$\omega_{n1} = \sqrt{\frac{k_t + c}{J}},\quad \omega_{n2} = \sqrt{\frac{k_t - c}{J}},$$

$$a_+ = \frac{M_c}{k_t + c},\quad \text{and}\quad a_- = \frac{M_c}{k_t - c}.$$

It is found that the natural frequency may vary due to the frictional torque. For example, if the initial condition $\phi_0 = 0.349$, $M_c = 10$ kg-mm, and $J = 0.01$ mm^4 are specified, the solution of first 2 cycles for the close-wound torsion spring in Table 2 becomes

$$\phi = (\phi_0 - a_-)\cos \omega_{n2}t + a_- \tag{22}$$

$$\dot{\phi} = -(\phi_0 - a_-)\omega_{n2}\sin \omega_{n2}t \tag{23}$$

$$\text{for}\quad 0 \leq t \leq \frac{\pi}{\omega_{n2}}$$

$$\phi = (-\phi_0 + 2a_- + a_+)\cos\left(\frac{\omega_{n1}\pi}{\omega_{n2}} - \omega_{n1}t\right) - a_+ \tag{24}$$

$$\dot{\phi} = (-\phi_0 + 2a_- + a_+)\omega_{n1}\sin\left(\frac{\omega_{n1}\pi}{\omega_{n2}} - \omega_{n1}t\right) \tag{25}$$
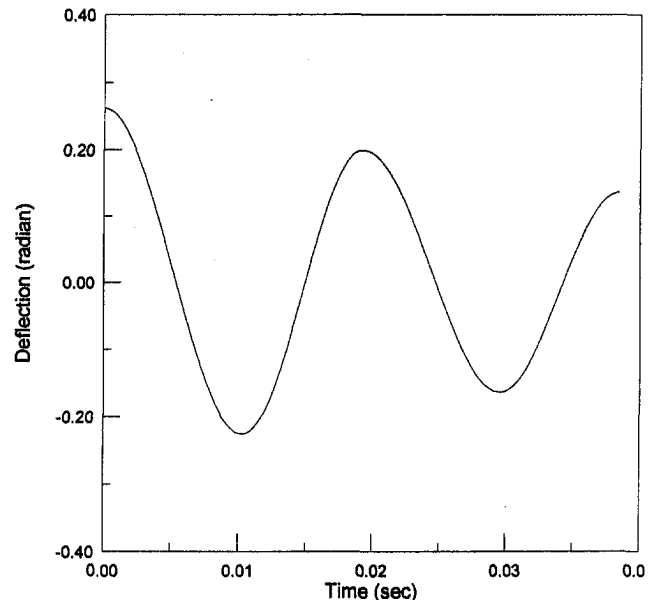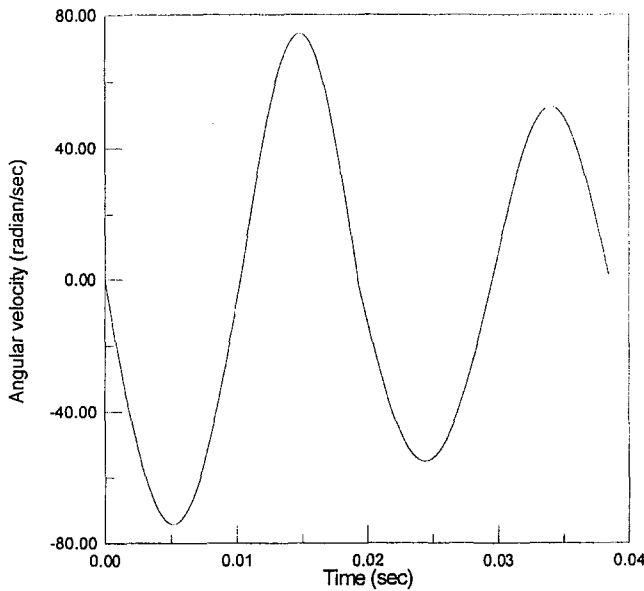

Fig. 10 Vibration of the close-wound torsion spring

Fig. 11 The angular velocity versus time

the friction torque is dependent on the deflection angle, the frequency $\omega_{n1} = 350.2825$ (rad/sec) in the load increasing stroke is larger than the frequency $\omega_{n2} = 305.2907$ (rad/sec) in the load decreasing stroke.

Conclusions

In the past, the moment-deflection relation was mostly assumed to be linear and the algorithm of determining the friction force for close-wound torsion spring was not discussed. Here a moment-deflection relationship is proposed and verified statically.

For the constant-pitch torsion spring without coil contact, it is found that only if the angular deflection is small, the linear theory is still acceptable. If the angular deflection is large, the effects of the inclined ends must be considered. It is found that the current theory can predict a larger stiffness by considering end effects, which is verified by experimental results, where the linear theory can not provide. For the close-wound torsion spring, the friction between the spring coils is critical to the performance of the torsion spring which has different spring rates between forward and backward stokes. Thus the natural frequency in the load increasing stroke is different from the natural frequency in the load decreasing stroke.

$$\text{for} \quad \frac{\pi}{\omega_{n2}} \leq t \leq \frac{\pi}{\omega_{n2}} + \frac{\pi}{\omega_{n1}}$$

$$\phi = (-\phi_0 + 3a_- + 2a_+) \cos\left(\frac{\omega_{n2}\pi}{\omega_{n1}} - \omega_{n2}t\right) + a_- \quad (26)$$

$$\dot{\phi} = (-\phi_0 + 3a_- + 2a_+)\omega_{n2} \sin\left(\frac{\omega_{n2}\pi}{\omega_{n1}} - \omega_{n2}t\right) \quad (27)$$

$$\text{for} \quad \frac{\pi}{\omega_{n2}} + \frac{\pi}{\omega_{n1}} \leq t \leq \frac{2\pi}{\omega_{n2}} + \frac{\pi}{\omega_{n1}}$$

$$\phi = (\phi_0 - 4a_- - 3a_+) \cos\left(\frac{2\pi\omega_{n1}}{\omega_{n2}} - \omega_{n1}t\right) - a_+ \quad (28)$$

$$\dot{\phi} = (\phi_0 - 4a_- - 3a_+)\omega_{n1} \sin\left(\frac{2\pi\omega_{n1}}{\omega_{n2}} - \omega_{n1}t\right) \quad (29)$$

$$\text{for} \quad \frac{2\pi}{\omega_{n2}} + \frac{\pi}{\omega_{n1}} \leq t \leq \frac{2\pi}{\omega_{n2}} + \frac{2\pi}{\omega_{n1}}$$

The simulated results are shown in Fig. 10 and Fig. 11. Because

References

1. Gohner, O., 1931, "Spannung sverteilung in einem an den Endquerschnitten belasteten Ringstabsektor," Ingenieur-Archiv, Vol. 2, pp. 406–411.
2. Gohner, O., 1938, "Zur Berechnung des gebogenen oder gedrillten Ringstabs mit Kreisquerschnitt und der zylindrischen Schraubenfeder," Ingenieur-Archiv, Vol. 9, pp. 356–363.
3. Berry, W. R., 1953, "An Investigation of Small Helical Torsion Springs," Proceedings (A), The Institution of Mechanical Engineers, Vol. 167, pp. 375–393.
4. Ancker, Jr., C. J., and Goodier, J. N., 1958, "Theory of Pitch and Curvature Corrections for the Helical Spring-II (Torsion)," ASME Journal of Applied Mechanics, Dec. pp. 484–495.
5. Ancker, Jr., C. J., and Goodier, J. N., 1958, "Pitch and Curvature Corrections for the Helical Spring," ASME Journal of Applied Mechanics, Dec. pp. 466–470.
6. Manos, T., 1956, "Variable Rate Torsion Spring," Ph.D. dissertation, University of Michigan, USA.
7. Carlson, H., 1979, "Squareness-Under-Load Testing and Buckling of Springs" ASME JOURNAL OF MECHANICAL DESIGN, Vol. 101, pp. 315–316.
8. Bruner, D. A., and Rouch, K., 1993, "Nonlinear Analysis of Springs Using Helical Finite Elements," Ph.D. dissertation, University of Kentucky, USA.
9. Wu, M. H., Ho, J. Y., and Hsu, W., 1997, "General Equations of a Helical Spring with a Cup Damper and Static Verification," ASME JOURNAL OF MECHANICAL DESIGN, Vol. 119, pp. 319–326.